

SIMULATIONS OF MAGNETOHYDRODYNAMIC TURBULENCE IN A STRONGLY MAGNETIZED MEDIUM

JUNGYEON CHO AND ALEX LAZARIAN

Department of Astronomy, University of Wisconsin, 475 North Charter Street, Madison, WI 53706; cho@astro.wisc.edu, lazarian@astro.wisc.edu

AND

ETHAN T. VISHNIAC

Department of Physics and Astronomy, Johns Hopkins University, 3400 North Charles Street, Baltimore, MD 21218; ethan@pha.jhu.edu

Received 2001 May 14; accepted 2001 September 4

ABSTRACT

We analyze three-dimensional numerical simulations of driven incompressible magnetohydrodynamic (MHD) turbulence in a periodic box threaded by a moderately strong external magnetic field. We sum over nonlinear interactions within Fourier wave bands and find that the timescale for the energy cascade is consistent with the Goldreich-Sridhar model of strong MHD turbulence. Using higher order longitudinal structure functions, we show that the turbulent motions in the plane perpendicular to the local mean magnetic field are similar to ordinary hydrodynamic turbulence, while motions parallel to the field are consistent with a scaling correction that arises from the eddy anisotropy. We present the structure tensor describing velocity statistics of Alfvénic and pseudo-Alfvénic turbulence. Finally, we confirm that an imbalance of energy moving up and down magnetic field lines leads to a slow decay of turbulent motions, and speculate that this imbalance is common in the interstellar medium, where injection of energy is intermittent both in time and space.

Subject headings: ISM: general — methods: numerical — MHD — turbulence

1. INTRODUCTION

The interstellar medium (ISM) is complicated and dynamic. The magnetic field and dynamic pressure ($\rho v^2/2$) usually dominate the thermal pressure (nkT), dramatically influencing the star formation rate (see McKee 1999 for a review). There are cosmic rays that provide pressure and heating as well.

One approach to studying the ISM is to perform time-dependent numerical simulations to model the ISM, including as many of the interacting phenomena as is practical. Of course, the physics included in such models must necessarily be highly simplified, and it is difficult to determine which features of the final model result from which physical assumptions (or initial conditions). Our approach is to use simplified numerical simulations for studying the influences of various physical phenomena in isolation. We want to obtain a physical feeling for the general effects that each phenomenon has on the nature of the ISM. In this paper, we consider the influence of random forces per unit volume on MHD turbulence in an incompressible medium. It is obvious that the real ISM is compressible, but we want to separate the effects of magnetic turbulence from those involving compression. In later papers, we will include compression for comparison with the present models, thereby isolating its importance directly.

Historically, hydrodynamic turbulence in an incompressible fluid was successfully described by the eddy cascade (Kolmogorov 1941), but MHD turbulence was first modeled by wave turbulence (Iroshnikov 1963; Kraichnan 1965; hereafter IK). This theory assumes isotropy of the energy cascade in Fourier space, an assumption that has attracted severe criticism (Montgomery & Turner 1981; Shebalin, Matthaeus, & Montgomery 1983; Montgomery & Matthaeus 1995; Sridhar & Goldreich 1994). Indeed, the magnetic field defines a local symmetry axis, since it is easy to mix field lines in directions perpendicular to the local \mathbf{B}

and much more difficult to bend them. The idea of an anisotropic (perpendicular) cascade has been incorporated into the framework of the reduced MHD approximation (Strauss 1976; Rosenbluth 1976; Montgomery 1982; Zank & Matthaeus 1992; Bhattacharjee, Ng, & Spangler 1998).

In a turbulent medium, the kinetic energy associated with large-scale motions is greater than that of small scales. However, the strength of the local mean magnetic field is almost the same on all scales. Therefore, it becomes relatively difficult to bend magnetic field lines as we consider smaller scales, leading to more pronounced anisotropy. A self-consistent model of MHD turbulence that incorporates this concept of scale-dependent anisotropy was introduced by Goldreich & Sridhar (1995, hereafter GS95).

Within the GS95 theory, the energy cascade becomes anisotropic as a consequence of the resonant conditions for three-wave interactions. A strict application of the resonant three-wave interaction conditions gives an energy cascade that is purely in the direction perpendicular to the external field. However, it is intuitively clear that the increase in k_{\perp} must at some point start affecting k_{\parallel} .

The cornerstone of the GS95 theory is the concept of a “critically balanced” cascade, where $k_{\parallel} V_A \sim k_{\perp} v_l$, k_{\perp} and k_{\parallel} are wavenumbers perpendicular and parallel to the background field, respectively, v_l is the rms speed of turbulence at the scale l and V_A is the Alfvén speed. In this model, the Alfvén rate ($k_{\parallel} V_A$) is equal to the eddy turnover rate ($k_{\perp} v_l$).

Using this concept, GS95 showed that the energy cascade is not strictly perpendicular to the background field, but is relaxed, so that $k_{\parallel} \propto k_{\perp}^{2/3}$.

Their model predicts that the one-dimensional energy spectrum is of Kolmogorov-type if expressed in terms of perpendicular wavenumbers, i.e., $E(k_{\perp}) \propto k_{\perp}^{-5/3}$.

Numerical simulations by Cho & Vishniac (2000a, hereafter CV00) and Maron & Goldreich (2001, hereafter MG01) have mostly supported the GS95 model and helped

to extend it. Both analyses stressed the point that scale-dependent anisotropy can be measured only in local coordinate frames that are aligned with the locally averaged magnetic field direction. CV00 calculated the structure functions of the velocity and magnetic field in the local frames, and found that the contours of the structure functions do show scale-dependent anisotropy, consistent with the predictions of the GS95 model. In their calculation, the strength of the uniform background magnetic field is roughly the same as the rms velocity. MG01 tested the GS95 model for a much stronger uniform background field and also obtained results supporting the GS95 model, but they produced $E(k) \propto k^{-3/2}$. They also calculated timescales of turbulence, interactions between pseudo- and shear-Alfvénic modes, growth of imbalance, and intermittency. Other related recent numerical simulations include Matthaeus et al. (1998), Müller & Biskamp (2000), and Milano et al. (2001).

These studies left a number of unresolved issues, including the exact scaling relations, the comparison of intermittency in MHD and in hydrodynamic turbulence, and the timescale of turbulence decay. Moreover, for many practical applications, a more quantitative description of MHD turbulence statistics is necessary. These are vital for understanding various astrophysical processes, including star formation (McKee 1999), cosmic-ray propagation (Kóta & Jokipii 2000), and magnetic reconnection (Lazarian & Vishniac 1999).

In this paper, we further investigate implications of the GS95 model. In § 2 we explain our numerical method. In § 3 we further elucidate the scaling relation implied by the GS95 model. In particular, we discuss the timescale, velocity scaling relations, and intermittency. In § 4 we derive the correlation tensor and discuss some astrophysical applications. While the GS95 model predicts that the MHD turbulence decays in just one eddy turnover time, in § 5 we show that the decay timescale increases when the cascade is unbalanced and discuss some consequences of this fact. In § 6 we briefly discuss the implications of this work. In § 7 we give a summary and our conclusions. As before, we consider the case in which the uniform background magnetic field energy density is comparable to the turbulent energy density.

2. METHOD

2.1. Numerical Method

We have calculated the time evolution of incompressible magnetic turbulence subject to a random driving force per unit mass. We have adopted a pseudospectral code for solving the incompressible MHD equations in a periodic box of size 2π :

$$\frac{\partial \mathbf{v}}{\partial t} = -(\nabla \times \mathbf{v}) \times \mathbf{v} + (\nabla \times \mathbf{B}) \times \mathbf{B} + \nu \nabla^2 \mathbf{v} + \mathbf{f} + \nabla P', \quad (1)$$

$$\frac{\partial \mathbf{B}}{\partial t} = \nabla \times (\mathbf{v} \times \mathbf{B}) + \eta \nabla^2 \mathbf{B}, \quad (2)$$

$$\nabla \cdot \mathbf{v} = \nabla \cdot \mathbf{B} = 0, \quad (3)$$

where \mathbf{f} is a random driving force, $P' \equiv P/\rho + \mathbf{v} \cdot \mathbf{v}/2$, \mathbf{v} is the velocity, and \mathbf{B} is the magnetic field divided by $(4\pi\rho)^{1/2}$. In this representation, \mathbf{v} can be viewed as the velocity mea-

sured in units of the rms velocity v of the system, and \mathbf{B} as the Alfvén speed in the same units. The time t is in units of the large eddy turnover time ($\sim L/v$), and the length is in units of L , the inverse wavenumber of the fundamental box mode. In this system of units, the viscosity ν and magnetic diffusivity η are the inverse of the kinetic and magnetic Reynolds numbers, respectively. The magnetic field consists of the uniform background field and a fluctuating field: $\mathbf{B} = \mathbf{B}_0 + \mathbf{b}$. We use 21 forcing components with $2 \leq k \leq (12)^{1/2}$, where the wavenumber k is in units of L^{-1} . Each forcing component has a correlation time of one. The peak of energy injection occurs at $k \approx 2.5$. The amplitudes of the forcing components are tuned to ensure $v \approx 1$. We use exactly the same forcing terms for all simulations. The Alfvén velocity of the uniform background field, B_0 , is set to 1. We consider only cases in which viscosity is equal to magnetic diffusivity:

$$\nu = \eta. \quad (4)$$

In pseudospectral methods, the temporal evolution of equations (1) and (2) are followed in Fourier space. To obtain the Fourier components of nonlinear terms, we first calculate them in real space and then transform back into Fourier space. The average kinetic helicity in these simulations is not zero. However, previous tests have shown that our results are insensitive to the value of the kinetic helicity. In an incompressible fluid, P' is not an independent variable. We use an appropriate projection operator to calculate the $\nabla P'$ term in Fourier space and also to enforce the divergence-free condition ($\nabla \cdot \mathbf{v} = \nabla \cdot \mathbf{B} = 0$). We use up to 256^3 collocation points. We use an integration factor technique for kinetic and magnetic dissipation terms and a leap-frog method for nonlinear terms. We eliminate the $2\Delta t$ oscillation of the leap-frog method by using an appropriate average. At $t = 0$, the magnetic field has only its uniform component, and the velocity field is restricted to the range $2 \leq k \leq 4$ in wavevector space.

Hyperviscosity and hyperdiffusivity are used for the dissipation terms (see Table 1). The power of the hyperviscosity is set to 8, so that the dissipation term in the above equation is replaced with

$$-v_8(\nabla^2)^8 \mathbf{v}, \quad (5)$$

where v_8 is determined from the condition $v_8(N/2)^{2h} \Delta t \approx 0.5$ (see Borue & Orszag 1996). Here Δt is the time step, and N is the number of grid points in each direction. The same expression is used for the magnetic dissipation term. We list the parameters used for the simulations in Table 1. We use the notation $XY-B_0Z$, where $X = 144$ or 256 refers to the number of grid points in each spatial direction, $Y = H$ refers to hyperviscosity, and $Z = 1$ refers to the strength of the external magnetic field.

Diagnostics for our code can be found in Cho & Vishniac (2000b). For example, our code conserves total energy very

TABLE 1
PARAMETERS

Run ^a	N^3	ν	η	B_0
144H-B ₀ 1.....	144 ³	3.20×10^{-28}	3.20×10^{-28}	1
256H-B ₀ 1.....	256 ³	6.42×10^{-32}	6.42×10^{-32}	1

^a For 256³ (or 144³) grids, we use the notation 256X-Y (or 144X-Y), where $X = H$ or P refers to hyper- or physical viscosity; $Y = B_0$ 1 refers to the strength of the external magnetic fields.

well in simulations with $\nu = \eta = 0$, and the average energy input ($= \mathbf{f} \cdot \mathbf{v}$) is almost exactly the same as the sum of magnetic and viscous dissipation in simulations with nonzero ν and η . The runs 256H- B_0 1 and 144H- B_0 1 are exactly the same as the runs 256H- B_0 1 and REF2 in CV00. The energy spectra as a function of time for these runs can be found in that paper.

2.2. Defining the Local Frame

The GS95 model deals with strong MHD turbulence and should be distinguished from theories that deal with weak MHD turbulence (e.g., Sridhar & Goldreich 1994; Ng & Bhattacharjee 1996; Galtier et al. 2000; see also Goldreich & Sridhar 1997). In strong MHD turbulence, eddy-like motions mix up magnetic field lines perpendicular to the local direction of the magnetic field. Thus, as in the case of hydrodynamic turbulence, the correlation time for coherent structures is comparable to the inverse of $k_{\perp} v_k$ for any scale k_{\perp}^{-1} . These mixing motions are strongly coupled to wavelike motions with a correlation time $(k_{\parallel} V_A)^{-1}$. The GS95 model is based on the concept of a critical balance between these timescales, that is, $k_{\parallel} V_A \sim k_{\perp} v_k$. This results in a scale-dependent anisotropy, $k_{\parallel} \propto k_{\perp}^{2/3}$, so that the eddies are increasingly elongated on smaller scales.

The turbulent magnetic field changes its direction in the *global* system of reference. It is important that the mixing motions are available only in the direction perpendicular to the *local* direction of magnetic field. Thus, the theory must be formulated using the system of reference aligned with the local magnetic field. CV00 discusses in detail one way of defining this system, given numerical data.

Figure 1 is a schematic representation of the GS95 model.¹ In Fourier space, the energy injected on large scales excites large-scale Fourier components of the magnetic field (the dark region at the center in Fig. 1a). The external mag-

netic field makes the subsequent energy cascade to small scales anisotropic: it occurs in the directions perpendicular to the mean external field.

The GS95 model states that most of the energy is confined to the region $k_{\parallel} = \pm k_{\perp}^{2/3}$, and as the energy cascades to larger values of k_{\perp} , the energy of the Fourier components between k_{\perp} and $k_{\perp} + 1$ decreases as $E(k_{\perp}) \propto k_{\perp}^{-5/3}$.

As illustrated in Figure 1b, eddies are not aligned along the mean field \mathbf{B}_0 . Instead, they are aligned along the *local mean* field lines. The local mean magnetic field defines the physically relevant background for the eddy dynamics and is determined by the Fourier components whose wavenumbers are a bit less than the characteristic wavenumber of the eddy. In practice, it can be obtained by averaging the magnetic field in the vicinity of the eddy over a volume slightly (for example, 2 times) larger than the size of the eddy (see CV00 for details). The solid curves in Figure 1b represent this kind of locally defined mean, formed by all magnetic Fourier components whose scales are a bit larger than eddy 1 (or 1'). The characteristic scale of this wandering is $L \sim 1/k_L$, the energy injection scale, because eddy 1 (or 1') is only slightly smaller than the energy injection scale. This large-scale wandering is smooth, but dominates over smaller scale effects because the magnetic energy is concentrated on larger scales. Wandering by smaller scale magnetic fields is weaker and causes smaller deviations from the large-scale wandering. We depict the additional wandering caused by scales a bit larger than eddy 2 as a dashed curve in Figure 1b. For eddy 1, the solid curve defines the local mean magnetic field, and for eddy 2, the dashed curve.

The GS95 model is dominated by local dynamics; that is, in this model, disturbances lose their coherence when propagating over a single wavelength. To the extent that the dynamics are local, it is obvious that the only relevant magnetic field is the local mean field. As an example, consider eddies 1 and 2 in Figure 1b again. For eddy 1, the solid curve can be regarded as a local mean field line, and the

¹ Note that Fig. 1 is *local frame* representation of the GS95 model. See below for more details.

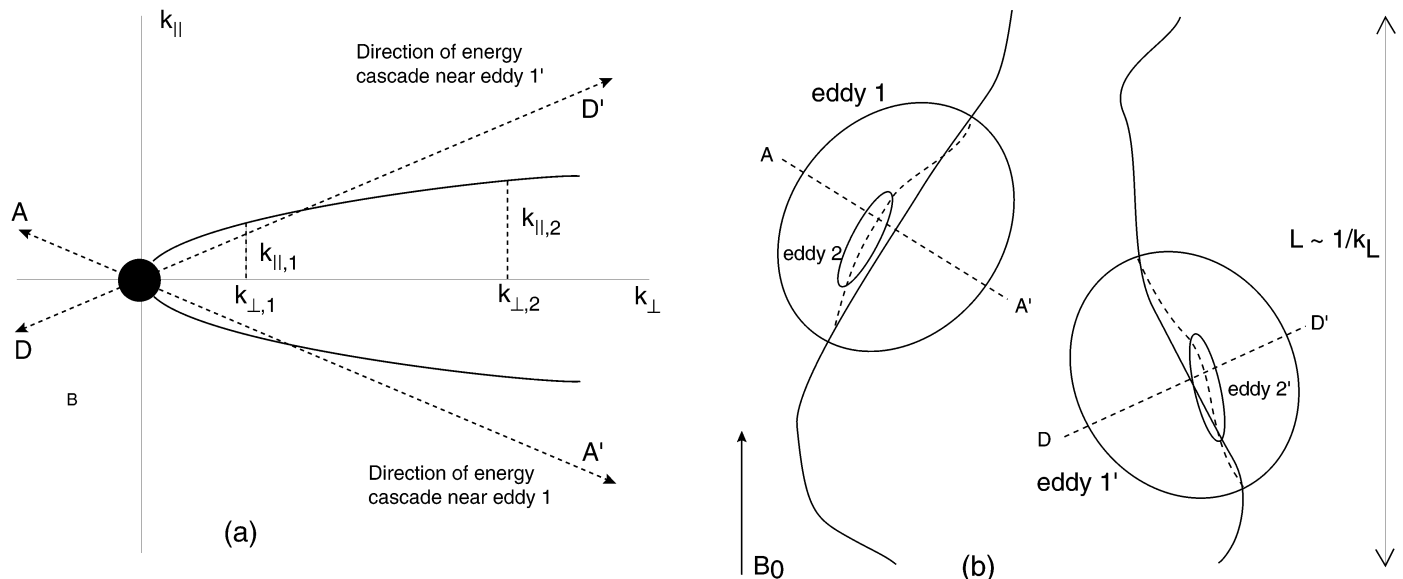


FIG. 1.—(a) Fourier-space structure. (b) Real-space structure. Large eddies (eddy 1 or 1') have similar semimajor axes ($\sim 1/k_{\parallel,1}$) and semiminor axes ($\sim 1/k_{\perp,1}$). Therefore, they are almost isotropic. Smaller eddies (eddy 2 or 2') have a relatively larger semimajor axis ($\sim 1/k_{\parallel,2}$)–semiminor axis ($\sim 1/k_{\perp,2}$) ratio. Therefore, they are relatively more elongated. Energy cascades in the directions perpendicular to large-scale magnetic field lines (e.g., direction AA' or DD' in both [a] and [b]). This effect obscures scale-dependent anisotropy (e.g., $k_{\parallel} \propto k_{\perp}^{2/3}$ in the GS95 model) when we perform Fourier analysis in the global frame. In (b), the solid curves represent the wandering of magnetic field lines by the large-scale magnetic fields. The solid curves can define the directions of the local mean magnetic field line for eddy 1 or 1'. Similarly, the dashed curves can define the directions of the local mean magnetic field line for the eddy 2 or 2'.

energy cascade takes place perpendicular to this field, along the direction AA' . Smaller eddies, such as eddy 2, see the dashed curve as their local background magnetic field, with a slightly different direction for the energy cascade. Since the difference between the two curves is small, the direction of the energy cascade differs only slightly as a function of scale. Basically, energy cascades along AA' in the region near eddy 1. Similarly, energy cascades along DD' in the region near eddy 1'. We are left with an energy cascade that differs both as a function of scale and as a function of location. However, the dynamics are *not* entirely local, in the sense that disturbances do propagate along field lines without retaining phase coherence. Consequently, perpendicular motions in eddy 1 can lead to similar motions in eddy 1', even though AA' and DD' are not parallel vectors. This is one of the key features of the GS95 model, and carried with it is the implication that dynamic variables need to be evaluated in terms of the local mean field direction, rather than a global coordinate system. Conversely, the ability to generate a more meaningful description in terms of a local and scale-dependent coordinate system can be taken as an indirect confirmation of some features of the GS95 model.

In summary, when we want to describe the scaling of eddy shapes, we should correctly identify the direction of the local mean magnetic field. When we talk about anisotropy, we talk about anisotropy with respect to local mean magnetic field lines. Because of this, it is necessary to introduce a “local” frame in which the direction of the local mean magnetic field lines is taken as the parallel direction. When we consider the GS95 picture (i.e., $k_{\parallel} \propto k_{\perp}^{2/3}$) in Fourier space, we are considering the *local* frame in real space, and vice versa. When we describe turbulence with respect to the *global* frame, which is fixed in real space, the corresponding Fourier-space structure no longer shows the GS95 picture. Instead, we have a relation close to $k_{\parallel} \propto k_{\perp}$. This is because when energy cascades along AA' , DD' , or some intermediate direction in real space (Fig. 1b), it cascades along the directions between AA' and DD' in Fourier space (Fig. 1a), which implies that when we perform the Fourier transform with respect to the fixed global frame,² we get $k_{\parallel} \propto k_{\perp}$. The true scaling relation is eclipsed by the wandering of large-scale magnetic field lines.

It is very important to identify the *local* frame. In this paper, when we calculate decay timescale, intermittency, and the correlation tensor, we always refer to the local frame.

3. SCALING RELATIONS

3.1. Timescale of Motions

One of the basic questions in the theory of MHD turbulence is the slope of the one-dimensional energy spectra. As we have seen, GS95 obtained a spectral index of $-5/3$. In the numerical simulations of CV00, the spectral index is close to $-5/3$, while it is very close to $-3/2$ in MG01. The IK theory predicts a $k^{-3/2}$ scaling, although the other features of this model are definitely inconsistent with all the numerical evidence. MG01 attributed their result to the appearance of strong intermittency in their simulations. We note that the inertial range of the solar wind shows a spec-

tral index of -1.7 (Leamon et al. 1998; see also Matthaeus & Goldstein 1982), but this number should be considered cautiously. The physics of the solar wind is undoubtedly more complicated than the simulations described here.

Can we test which scaling is correct? The cascade time as a function of scale presents us with an interesting constraint.

The IK theory and GS95 model predict different scalings for the turbulent cascade timescale (t_{cas}). In both theories, t_{cas} can be determined by the scale-independence of the cascade:

$$v_k^2/t_{\text{cas}} = \text{const} . \quad (6)$$

Since v_k^2 is proportional to $kE(k)$, we have

$$t_{\text{cas,IK}} \propto k^{-1/2} , \quad t_{\text{cas,GS}} \propto k^{-2/3} \quad (7)$$

for the IK theory and GS95 model, respectively. This result is also useful for certain intermittency theories (see § 3.3). MG01 studied the cascade timescale using three different methods and obtained slopes comparable to $-2/3$ (i.e., $t_{\text{cas}} \propto k_{\perp}^{-2/3}$) in two methods and $-1/2$ in the other method.

Here we consider a different method of evaluating t_{cas} . The purpose of our calculation is to test MG01's result using another numerical method and demonstrate the effects of large-scale fluid motions on the calculation of t_{cas} .

Symbolically, we can rewrite the MHD equations as

$$\dot{\mathbf{v}}_k = N_k^v , \quad (8)$$

$$\dot{\mathbf{b}}_k = N_k^b , \quad (9)$$

where N^v and N^b represent nonlinear terms. We have ignored the dissipation terms. Naively, we might obtain the timescale by dividing $|\mathbf{v}_k|$ by $|N_k^v|$. However, this gives $t_{\text{cas}} \propto k^{-1}$, where the exponent is almost exactly -1 . This is not actually a measure of the cascade time. We note that CV00 obtained a similarly misleading relation for the cascade time and attributed it to the effect of large-scale translational motions. Although they used a different method for calculating the cascade time, the same argument applies here. If we consider the interaction between a small eddy and a large-scale (translational) fluid motion, then the translation can be removed by a Galilean transformation, and there is no associated energy cascade. However, the phase of the Fourier components that represent the small eddy is affected by the large-scale translational motion and changes at a rate kV , where V is the large-scale velocity. The corresponding nonlinear term has a magnitude of $|N_k| \sim |\mathbf{v}_k|kV$, which accounts for the (misleading) relation $t_{\text{cas}} \sim k^{-1}$. The cascade time as a function of wavenumber can be evaluated directly from our simulations, but only after we filter out translational motions arising from eddies much larger than the scale under consideration.

We correct for the presence of large-scale motions by restricting the evaluation of the nonlinear terms to contributions coming from the interactions between the mode at k and other modes within the range³ of $k/2-2k$. In doing this, we retain the uniform magnetic component B_0 . We show the result in Figure 2. Our result supports the GS95 model: $t_{\text{cas}} \propto k^{-2/3}$. In comparison with MG01, we obtained this result using a different method and for a different kinetic/magnetic energy ratio.

In the GS95 model, t_{cas} is determined by the relation $t_{\text{cas}} \sim l_{\perp}/v_{l_{\perp}}$. This means that the cascade timescale is vir-

² Many astrophysical observations, for instance, interferometric observations of turbulent H I (Lazarian 1995), provide the statistics measured in the global frame.

³ This assumes some sort of locality, which may not be exact in the presence of strong intermittency.

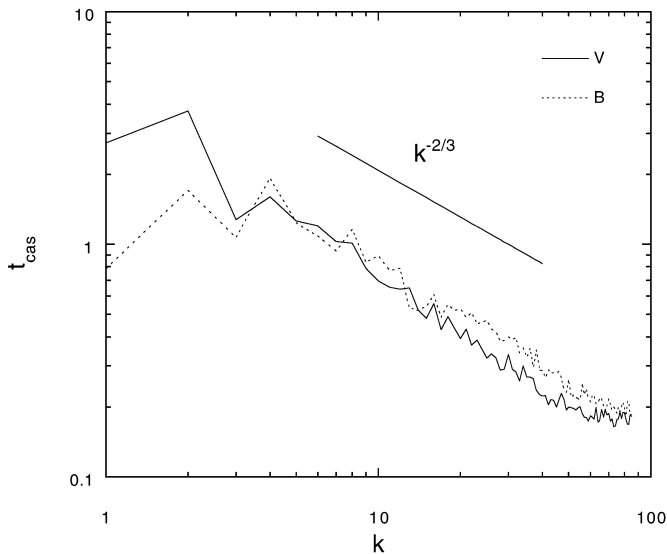


FIG. 2.—Cascade timescale for run 256H-B₀1. The GS95 model predicts $t_{\text{cas}} \propto k^{-2/3}$, while the IK theory predicts $t_{\text{cas}} \propto k^{-1/2}$. Our result supports the GS95 model.

tually synonymous with the eddy turnover time, which is also true for hydrodynamic turbulence. It is obvious that the cascade time determines the decay timescale of turbulence. As a consequence, the GS95 model implies that MHD turbulence decays as fast as hydrodynamic turbulence (e.g., $t_{\text{decay}} = \text{a few eddy turnover times}$). Note that no matter how strong the external field is, strong MHD turbulence decays within a few eddy turnover times. We discuss the implications of this result, and some limitations, in § 5.

These results support the original GS95 theory. However, we are not in a position to directly confront the results of MG01. Our simulations differ from theirs in many ways, including the shape of the computational box, the range of length scales, and the strength of the uniform background field. We will address those issues elsewhere. In § 3.3 we discuss what the study of intermittency implies about the slope of energy spectra.

3.2. Velocity Scaling

In the GS95 model, v_{\perp}^2 is proportional to $\sim k_{\perp} E(k_{\perp})$, where $E(k_{\perp})$ is the one-dimensional energy spectrum. Since $E(k_{\perp}) \propto k_{\perp}^{-5/3}$, we have $v_{\perp}^2 \propto l_{\perp}^{2/3}$, or $\text{SF}_2(l_{\perp}, 0) \propto l_{\perp}^{2/3}$, where SF_2 is the second-order structure function:

$$\text{SF}_2(l_{\perp}, l_{\parallel}) = \langle [\mathbf{v}(\mathbf{x} + \mathbf{l}) - \mathbf{v}(\mathbf{x})]^2 \rangle, \quad (10)$$

where the angle brackets denote the spatial average over \mathbf{x} and $\mathbf{l} = l_{\perp} \mathbf{e}_{\perp} + l_{\parallel} \mathbf{e}_{\parallel}$. The vectors \mathbf{e}_{\perp} and \mathbf{e}_{\parallel} are unit vectors perpendicular and parallel to \mathbf{B}_L , respectively. The vector \mathbf{B}_L denotes the local mean magnetic field.

What can we say about the velocity scaling parallel to \mathbf{B}_L ? We can consider two different quantities. First, we can consider the scaling of Alfvén components in the direction parallel to \mathbf{B}_L . Second, we can also consider the scaling of pseudo-Alfvénic components along the direction of \mathbf{B}_L . The pseudo-Alfvénic components are the incompressible limit of slow magnetosonic waves. While they have the same dispersion relations as the Alfvén modes, the velocities v_l of polarization are completely different: the directions lie in the plane determined by \mathbf{B}_0 and \mathbf{k} . Note that the Alfvén modes have velocities perpendicular to the plane determined by \mathbf{B}_0 and \mathbf{k} .

There are several ways to derive the scaling relation for Alfvénic turbulence from the GS95 model. First, suppose that the second-order structure function along local \mathbf{B}_L follows a power law: $\text{SF}_2(0, l_{\parallel}) \propto l_{\parallel}^m$.

When we equate $\text{SF}_2(0, l_{\parallel})$ and $\text{SF}_2(l_{\perp}, 0)$, we should retrieve the GS95 scaling relation, $l_{\parallel} \propto l_{\perp}^{2/3}$ (see MG01). We conclude that $m = 1$ and $\text{SF}_2(0, l_{\parallel}) \propto l_{\parallel}$. Since $k_{\parallel} E^v(k_{\parallel}) \propto v_{\parallel}^2 \propto \text{SF}_2(l_{\parallel}, 0)$, we have $E^v(k_{\parallel}) \propto k_{\parallel}^{-2}$. Alternatively, we can write

$$E_3^v(k_{\perp}, k_{\parallel}) \propto k_{\perp}^{-10/3} g(k_{\parallel}/k_{\perp}^{2/3}), \quad (11)$$

where $E_3^v(k_{\perp}, k_{\parallel})$ is the three-dimensional energy spectrum and g is a function that describes distribution of energy along the k_{\parallel} direction in Fourier space. We give a reasonable fit to its functional form in the next section.

We plot our results in Figure 3, in which we observe that $\text{SF}_2(l_{\perp}, 0)$ (across \mathbf{B}_L) $\propto l_{\perp}^{2/3}$ and $\text{SF}_2(0, l_{\parallel})$ (parallel to \mathbf{B}_L) $\propto l_{\parallel}$. The velocity field follows these relations quite well, while the magnetic field follows a slightly different relation across \mathbf{B}_L . Both Alfvénic and pseudo-Alfvénic components follow similar scalings in the directions parallel to \mathbf{B}_L . In § 4 we also show that the three-dimensional spectrum of pseudo-Alfvén motions has a form similar to equation (11). On this basis, we conclude that the scaling $E^v(k_{\parallel}) \propto k_{\parallel}^{-2}$ also applies to pseudo-Alfvén motions, where the velocities are mostly parallel to the local mean magnetic field \mathbf{B}_L . The corresponding velocities $v_{\parallel}^2 \propto k_{\parallel} E^v(k_{\parallel})$, which means that $v_{\parallel}^2 \propto k_{\parallel}^{-1} \propto l_{\parallel}$. This result is important for many problems, including dust transport (H. Yan et al., in preparation). Note that the energy spectrum is steeper when expressed as a function of the parallel direction.

In this subsection we extended the GS95 model for the parallel motions and pseudo-Alfvén modes and confirmed it through numerical simulations.

3.3. Intermittency

MG01 studied the intermittency of dissipation structures in MHD turbulence using the fourth-order moments of the

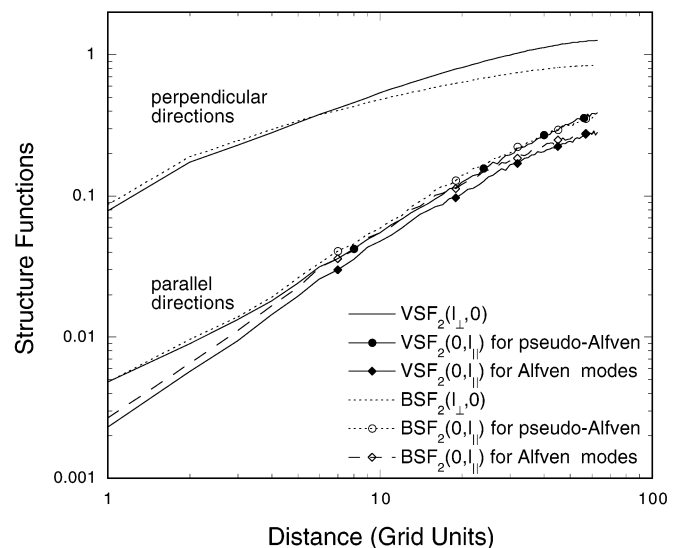


FIG. 3.—Second-order structure functions for run 256H-B₀1. Across local mean magnetic field lines, the second-order structure functions follow $r^{2/3}$. Along the local mean magnetic field lines, they follow r^1 . For pseudo-Alfvén modes, this defines the scaling of motions parallel to local mean magnetic field lines. The terms VSF₂ and BSF₂ denote the second-order structure functions for the velocity and magnetic fields, respectively.

Elsasser fields and the gradients of the fields. Their simulations show strong intermittent structures. We use a different, but complementary, method for studying intermittency, based on the higher order longitudinal structure functions. Our result is that by this measure, the intermittency of the velocity field in MHD turbulence across local magnetic field lines is as strong as, but not stronger than, in hydrodynamic turbulence.

In fully developed hydrodynamic turbulence, the (longitudinal) velocity structure functions $S_p = \langle \{[\mathbf{v}(\mathbf{x} + \mathbf{r}) - \mathbf{v}(\mathbf{x})] \cdot \hat{\mathbf{r}}\}^p \rangle \equiv \langle \delta v_L^p(r) \rangle$ are expected to scale as $r^{p/3}$. For example, the classical Kolmogorov (1941) phenomenology predicts $\zeta_p = p/3$. The (exact) result for $p = 3$ is the well-known $4/5$ relation: $\langle \delta v_L^3(r) \rangle = -(4/5)\epsilon r$, where ϵ is the energy injection rate (or energy dissipation rate). On the other hand, She & Leveque (1994, hereafter SL94) proposed a different scaling relation: $\zeta_p^{\text{SL}} = p/9 + 2[1 - (2/3)^{p/3}]$. Note that She-Leveque model also implies $\zeta_3 = 1$.

So far in MHD turbulence, to the best of our knowledge, there is no rigorous intermittency theory that takes into account scale-dependent anisotropy. Therefore, we use an intermittency model based on an extension of a hydrodynamic model. Politano & Pouquet (1995) have developed an MHD version of the She-Leveque model:

$$\zeta_p^{\text{PP}} = \frac{p}{g} (1 - x) + C \left[1 - \left(1 - \frac{x}{C} \right)^{p/g} \right], \quad (12)$$

where C is the codimension of the dissipative structure, g is related to the scaling, $v_l \sim l^{1/g}$, and x can be interpreted as the exponent of the cascade time $t_{\text{cas}} \propto l^x$. (In fact, g is related to the scaling of the Elsasser variable z : $z_l \sim l^{1/g}$.) In the framework of the IK theory, where $g = 4$, $x = \frac{1}{2}$, and $C = 1$ when the dissipation structures are sheetlike, their model of intermittency becomes $\zeta_p^{\text{IK}} = p/8 + 1 - (1/2)^{p/4}$. On the other hand, Müller & Biskamp (2000) performed numerical simulations on decaying isotropic MHD turbulence and obtained Kolmogorov-like scaling [$E(k) \sim k^{-5/3}$ and $t \sim l^{2/3}$] and sheetlike dissipation structures, which implies $g = 3$, $C = 1$, and $x = \frac{2}{3}$. From equation (12), they

proposed that

$$\zeta_p^{\text{MB}} = p/9 + 1 - (1/3)^{p/3}. \quad (13)$$

How does anisotropy change intermittency? We determined the scaling exponents numerically, working in the local frame. We performed a simulation with a grid of 144^3 collocation points and integrated the MHD equations from $t = 75$ –120. We calculated the higher order velocity structure functions for 75 evenly spaced snapshots. We averaged over five consecutive values, since the correlation time of the turbulence corresponded to five snapshots. We calculated the scaling exponents from these averaged structure functions. We obtained a total of 15 (=75/5) such structure functions and scaling exponents. We believe that these 15 data sets are mutually independent. We plot the result in Figure 4 (*left panel*). The filled circles represent the scaling exponents of longitudinal velocity structure functions in directions *perpendicular* to the local mean magnetic field. It is surprising that the scaling exponents are close to the original (i.e., hydrodynamic) SL94 model. This raises an interesting question. In our simulations, we clearly observe that $t_{\text{cas}} \propto l^{2/3}$ and $E(k) \propto k^{-5/3}$. It is evident that MHD turbulence has sheetlike dissipation structures (Politano, Pouquet, & Sulem 1995). Therefore, the parameters for our simulations should be the same as those of Müller & Biskamp's (i.e., $g = 3$, $C = 1$, and $x = 2/3$), rather than suggesting $C = 2$. We believe that this difference stems from the different simulation settings: their turbulence is isotropic and ours is anisotropic. In fact, we expect that the small-scale behavior of MHD turbulence should not depend on whether or not the largest scale fields are uniform or have the same scale of organization as the largest turbulent eddies. Nevertheless, given the limited dynamical range available in these simulations, it would not be surprising if the scale of the magnetic field has a dramatic impact on the intermittency statistics. It is not clear how scale-dependent anisotropy changes the intermittency model in equation (12), and we do not discuss this issue further. Instead, we simply stress that we have found a striking similarity

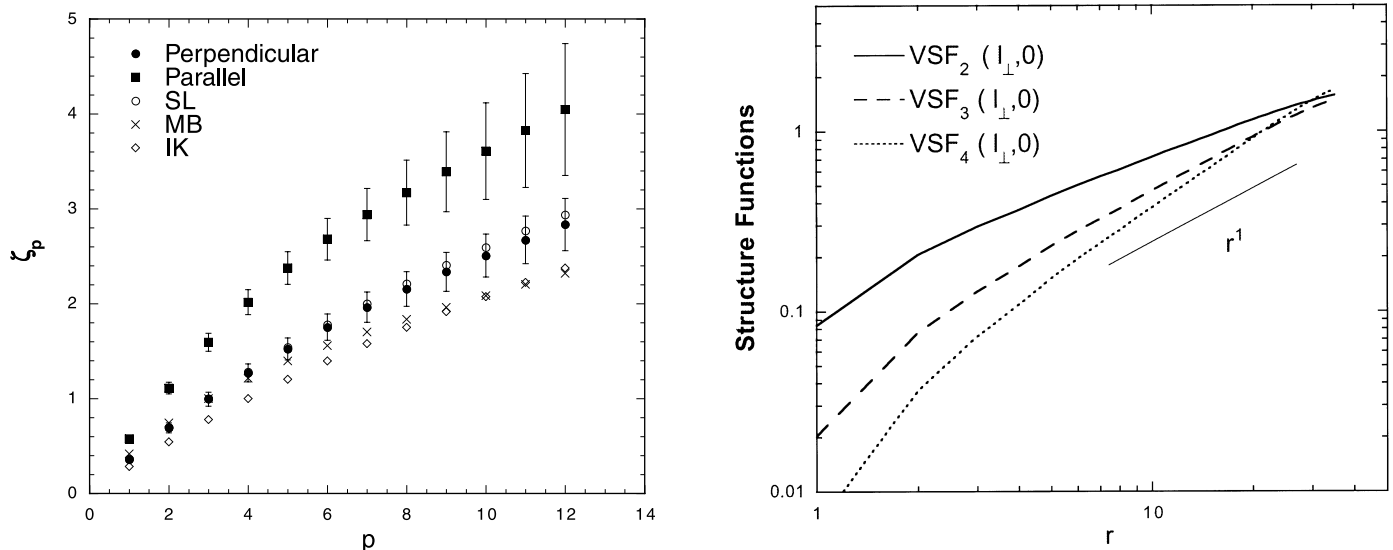


FIG. 4.—*Left*: Intermittency for run 144H-B₀1. Our result (*filled circles*) suggests that MHD turbulence looks like ordinary hydrodynamic turbulence when viewed across the local field lines. SL represents the original She-Leveque model for ordinary hydrodynamic turbulence. IK and MB stand for the IK theory and the Müller-Biskamp model, respectively. Error bars are for the 1σ level. *Right*: The second-, third-, and fifth-order longitudinal velocity structure functions. These are structure functions averaged over the time interval (75, 120).

between ordinary hydrodynamic turbulence and MHD turbulence in perpendicular directions. MG01 attributes the deviation of their spectrum from the Kolmogorov-type to the turbulence intermittency present in the MHD case. Since we do not reproduce their power spectrum, the fact that our intermittency statistics do not support this conjecture is unsurprising. Clearly, more studies of the issue are necessary.

In Figure 4 (*left panel*), we also plot the scaling exponents (represented by filled squares) of longitudinal velocity structure functions *along* directions of the local mean magnetic field. Although we show only the exponents of longitudinal structure functions, those of transverse structure functions follow a similar scaling law. It is evident that intermittency along the local mean magnetic field directions is completely different from that of previous (isotropic) models. Roughly speaking, the scaling exponents along the directions of the local magnetic field are 1.5 times larger than those of perpendicular directions. Interestingly, this result, which implies anisotropy, becomes scale independent under the following transformation: $(r_{\perp}, r_{\parallel}) \rightarrow (r_{\perp}, r_{\parallel}^{2/3})$. This is consistent with the idea that eddies are stretched along the directions of the local mean magnetic field; if we shrink them in the scale-dependent manner described above along the local field lines, the result is similar to ordinary hydrodynamic turbulence. In this interpretation, it is not surprising that MHD turbulence looks similar to ordinary hydrodynamic turbulence across the local mean magnetic field lines; the scaling relation in perpendicular directions is not affected by the local mean magnetic field. Clearly this result is difficult to explain using previous models, for example, the IK theory. The error bars are larger for parallel directions because a fewer number of pairs are available for calculation of the structure functions in these directions than in perpendicular directions.

In Figure 4 (*right panel*), we plot average longitudinal velocity structure functions. The slope of the third-order structure function is very close to 1. The third-order structure function is slightly different from the one discussed earlier in that we calculate $\langle |\delta v_L|^3(r) \rangle$ instead of $\langle (\delta v_L)^3(r) \rangle$.

The second-order exponent ζ_2 is related to the one-dimensional energy spectra: $E(k_{\perp}) \propto k_{\perp}^{-(1+\zeta_2)}$. Previous two-dimensional driven MHD calculations for $B_0 = 0$ by Politano, Pouquet, & Carbone (1998) also found $\zeta_2 \sim 0.7$. However, Biskamp & Schwarz (2001) obtained $\zeta_2 \sim 0.5$ from decaying two-dimensional MHD calculations with $B_0 = 0$. Our result suggests that ζ_2 is closer to $\frac{2}{3}$, rather than to $\frac{1}{2}$. (It is not clear whether or not the scaling exponents follow the original SL94 model exactly. At the same time, our calculation shows that the original SL94 model can be a good approximation for our scaling exponents. The SL94 model predicts that $\zeta_2 \sim 0.696$.) Therefore, our result supports the scaling law $E(k_{\perp}) \propto k_{\perp}^{-5/3}$, at least for velocity. For the parallel directions, the results support $E(k_{\parallel}) \propto k_{\parallel}^{-2}$, although the uncertainty is large.

4. THE MHD FLUCTUATION TENSOR

For many purposes, e.g., cosmic-ray propagation and acceleration, heat transfer, etc., it is necessary to know the tensor describing the statistics of the magnetic and velocity fields. For those applications, the one-dimensional spectrum described in MG01 is not adequate, and a more detailed description is necessary.

General second-rank correlation tensors are important tools in the statistical description of turbulence. Oughton, Radler, & Matthaeus (1997) gave a comprehensive formalism for the tensors for MHD turbulence, and we use their results as the starting point of our argument. Consider the velocity correlation tensor

$$R_{ij}^v = \langle v_i(x)v_j(x+r) \rangle, \quad (14)$$

where the angle brackets denote an appropriate ensemble average. The Fourier transform of this tensor is

$$S_{ij}^v = \langle \hat{v}_i(\mathbf{k})\hat{v}_j^*(\mathbf{k}) \rangle, \quad (15)$$

where the asterisk denotes the complex conjugate. We can rewrite equation (20) of Oughton et al. (1997) as

$$S_{ij}^v = \left(\delta_{ij} - \frac{k_i k_j}{k^2} \right) E^v(\mathbf{k}) + \left[(e_i k_j + e_j k_i)(e \cdot \mathbf{k}) - e_i e_j k^2 - \frac{k_i k_j}{k^2} (e \cdot \mathbf{k})^2 \right] F^v(\mathbf{k}) + X_{ij}, \quad (16)$$

where $E^v(\mathbf{k})$ is the (three-dimensional) kinetic energy spectrum of all (shear + pseudo) modes, $F^v(\mathbf{k})$ is the difference of shear-Alfvén energy and pseudo-Alfvén energy at wave vector \mathbf{k} divided by k^2 , e is a unit vector along \mathbf{B}_0 , and $X_{ij} = -i(\delta_{i\mu}\epsilon_{j\alpha\beta} + \delta_{j\mu}\epsilon_{i\alpha\beta})e_{\alpha}k_{\beta}(e_{\mu}k^2 - k_{\mu}e \cdot \mathbf{k})C^v + i\epsilon_{ij\alpha}k_{\alpha}H^v$ is a term that describes deviation from mirror symmetry. In this paper, we consider axisymmetric turbulence (caused by \mathbf{B}_0) with mirror symmetry, so that $X_{ij} \equiv 0$. We need only two scalar generating functions, E^v and F^v , for the correlation tensor. This is consistent with Chandrasekhar (1951; see also Oughton et al. 1997).

In this subsection, we show that the tensor is suitably described by

$$S_{ij} = A_1 \left(\delta_{ij} - \frac{k_i k_j}{k^2} \right) k_{\perp}^{-10/3} \exp \left(-A_2 \frac{k_{\parallel}}{k_{\perp}^{2/3}} \right), \quad (17)$$

where $A_1 \sim B_0^2/L^{1/3}$ and $A_2 \sim L^{1/3}$ are parameters.

First, we choose $e = (0,0,1)$, the direction of \mathbf{B}_0 . Then, equation (16) becomes

$$S_{ij}^v = \left(\delta_{ij} - \frac{k_i k_j}{k^2} \right) E^v(\mathbf{k}) + \left[(\delta_{3i} k_j + \delta_{3j} k_i) k_3 - \delta_{3i} \delta_{3j} k^2 - \frac{k_i k_j}{k^2} k_3^2 \right] F^v(\mathbf{k}). \quad (18)$$

In the absence of anomalous damping of the pseudo-Alfvén modes, as in our simulations, we can show that F in the above expression is negligibly small. Note that $F = (S - P)/k_{\perp}^2$, where S and P are the squares of the amplitudes of the shear- and pseudo-Alfvén modes (i.e., three-dimensional energy spectra). To evaluate S and P , we measured their strength in the global frame. (It is nontrivial to correctly define Alfvén modes and pseudo-Alfvén modes in the local frame.) Figure 5 shows that they have similar strengths. We assume that the same relation holds true in the local frame. Since F is the difference between S and P , it follows that $F(\mathbf{k})$ is small compared to $E(\mathbf{k})$.

In the previous paragraph, we assumed that there is no special damping mechanism for the pseudo-Alfvén modes. However, it is known that pseudo-Alfvén modes in the ISM are subject to strong damping due to free streaming of collisionless particles along the field lines (Barnes 1966; Minter & Spangler 1997). When the pseudo-Alfvén modes are

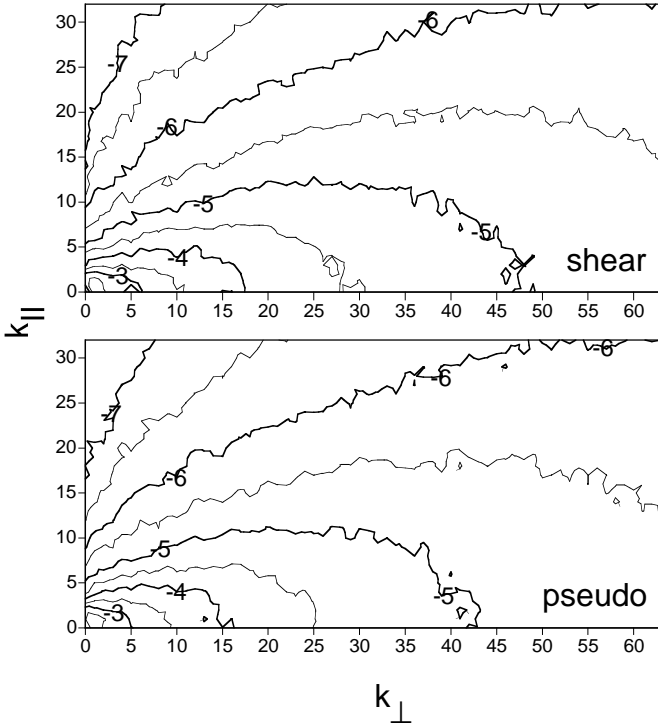


FIG. 5.—Energy distribution of shear- and pseudo-Alfvén waves for run 256H-B₀1. They have similar energy distributions in Fourier space (global frame). Numbers by the contours are $\log_{10} [E_3(k)]$.

absent, equation (16) becomes

$$S_{ij}^v = \left(\delta_{ij} - \frac{k_i k_j}{k^2} \right) E^v(\mathbf{k}) + \left[(\delta_{3i} k_j + \delta_{3j} k_i) k_3 - \delta_{3i} \delta_{3j} k^2 - \frac{k_i k_j}{k^2} k_3^2 \right] \frac{E^v(\mathbf{k})}{k_{\perp}^2}. \quad (19)$$

For $i, j = 1, 2$, this becomes $S_{ij} = (\delta_{ij} - k_i k_j / k^2) E - (k_i k_j / k^2) (k_{\parallel} / k_{\perp})^2 E \approx (\delta_{ij} - k_i k_j / k^2) E$, and it is easy to show that $S_{i3} = S_{3i} = 0$. This is easily understood when we note that shear Alfvén waves do not have fluctuations along B_0 .

In summary, the tensor reduces to

$$\begin{bmatrix} (1 - k_1^2/k^2)E & -(k_1 k_2/k^2)E & -(k_1 k_3/k^2)E \\ -(k_1 k_2/k^2)E & (1 - k_2^2/k^2)E & -(k_2 k_3/k^2)E \\ -(k_1 k_3/k^2)E & -(k_2 k_3/k^2)E & (1 - k_3^2/k^2)E \end{bmatrix} \quad (20)$$

for turbulence with both Alfvénic and pseudo-Alfvénic components, and

$$\begin{bmatrix} (1 - k_1^2/k^2)E & -(k_1 k_2/k^2)E & 0 \\ -(k_1 k_2/k^2)E & (1 - k_2^2/k^2)E & 0 \\ 0 & 0 & 0 \end{bmatrix} \quad (21)$$

for shear Alfvénic turbulence. In equation (21), E stands for the energy of Alfvén components only, which is roughly one-half of the E in equation (20).

The remaining issue is the form of E . Note that the trace of S_{ij}^v is $2E^v$. In real space, the trace is the velocity correlation function. Consequently, we can obtain E^v through a FFT of the real-space velocity correlation function, which is directly available from our data cube. However, the velocity correlation function in real space contains considerable

numerical noise. In order to minimize its effects while obtaining an empirically useful form for E , we first guess E^v in Fourier space, do the FFT transform, and then compare the transformed result with the actual velocity correlation function. Since the trace of S_{ij}^v is the (three-dimensional) energy spectrum in Fourier space, we start with the original expression in GS95, given by equation (11):

$$E_3(k_{\perp}, k_{\parallel}) \sim \frac{B_0^2}{k_{\perp}^{10/3} L^{1/3}} g\left(L^{1/3} \frac{k_{\parallel}}{k_{\perp}^{2/3}}\right), \quad (22)$$

where the functional form of $g(y)$ was not specified. We have tried several functional forms for g ; Gaussian [$g \propto \exp(-Bk_{\parallel}^2/k_{\perp}^{4/3})$], exponential [$\exp(-Bk_{\parallel}/k_{\perp}^{2/3})$], and a step function. We have found that an exponential form for g gives the best result (Fig. 6). Figure 6 (*top panel*) is the actual data that we obtained from our simulation, and Figure 6 (*bottom panel*) is the Fourier-transformed velocity correlation function. Note the similarity of the contours in both plots. We conclude that the tensor can be suitably described by equation (20) or (21), with

$$E(k_{\perp}, k_{\parallel}) = \left(\frac{B_0}{L^{1/3}} \right) k_{\perp}^{-10/3} \exp\left(-L^{1/3} \frac{k_{\parallel}}{k_{\perp}^{2/3}}\right), \quad (23)$$

where k_{\perp} and k_{\parallel} should both be interpreted as the absolute magnitudes of those wavevector components.

However, it is worth noting a clear limitation of equation (23): it has a discontinuous derivative near $k_{\parallel} = 0$. One way to overcome this difficulty is to use the Castaing function⁴

⁴ Our motivation for introducing the Castaing function is phenomenological, not theoretical. The theory of the distribution function for MHD turbulence is uncertain, and far beyond the scope of this paper.

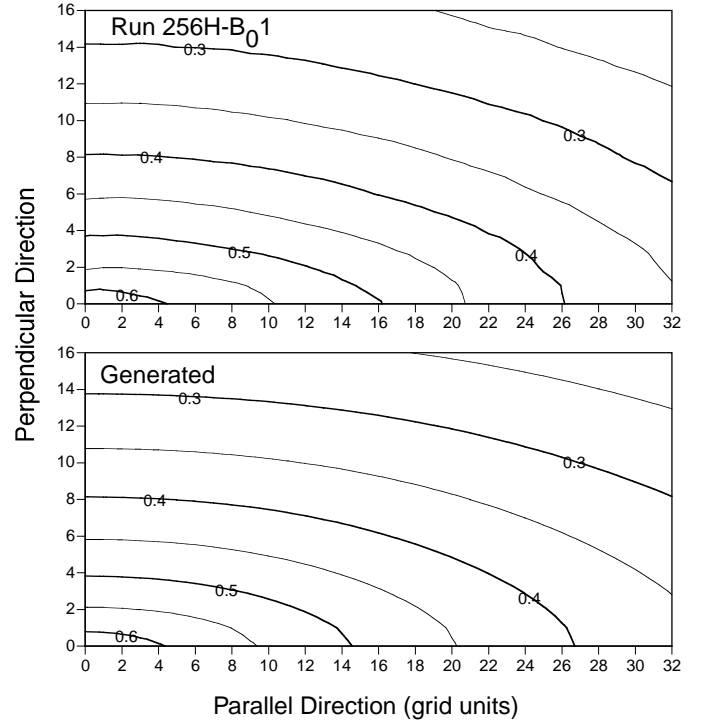


FIG. 6.—*Top*: Velocity correlation function from simulations. *Bottom*: Velocity correlation function generated using the tensor in eq. (23). Parallel and perpendicular directions are taken with respect to local mean magnetic field.

(Castaing, Gagne, & Hopfinger 1990)

$$\Pi_\lambda(u) = \frac{1}{2\pi\lambda} \int_0^\infty \exp\left(-\frac{u^2}{2\sigma^2}\right) \exp\left[-\frac{\ln^2(\sigma/\sigma_0)}{2\lambda^2}\right] \frac{d\sigma}{\sigma^2}, \quad (24)$$

which is smooth near zero, but looks exponential over a broad range. It is possible to see that for $\lambda = 1$ and $\sigma_0 = k_\perp^{2/3}/L^{1/3}$,

$$\exp\left(-L^{1/3} \frac{k_\parallel}{k_\perp^{2/3}}\right) \approx \frac{1}{2\pi} \int_0^\infty \exp\left(-\frac{k_\parallel^2}{2\sigma^2}\right) \times \exp\left[-\frac{\ln^2(L^{1/3}\sigma/k_\perp^{2/3})}{2}\right] \frac{d\sigma}{\sigma^2}. \quad (25)$$

However, for many practical applications, we feel that the expression in equation (23) is adequate. For instance, in a forthcoming paper (H. Yan et al., in preparation), this tensor is used for describing cosmic-ray propagation, and we find a strong suppression of cosmic-ray scattering compared with the generally accepted estimates (for example, Schlickeiser 1994). However, if the behavior around k_\parallel is important, the Castaing function would be preferred. In our simulations, there is no way to distinguish between exponential and Castaing distributions.

5. DECAY OF MHD TURBULENCE

Turbulence plays a critical role in molecular cloud support and star formation, and the issue of the timescale of turbulent decay is vital for understanding these processes.

If MHD turbulence decays quickly, then serious problems face researchers attempting to explain important observational facts, i.e., turbulent motions seen within molecular clouds without star formation (see Myers 1999) and rates of star formation (McKee 1999). Earlier studies attributed the rapid decay of turbulence to compressibility effects (Mac Low 1999). Our present study, as well as earlier ones (CV00; MG01), shows that turbulence decays rapidly, even in the incompressible limit. This can be understood in the framework of the GS95 model, in which mixing motions perpendicular to magnetic field lines form hydrodynamic-type eddies. Such eddies, as in hydrodynamic turbulence, decay in one eddy turnover time.

How grave is this problem? Some possibilities for reconciling theory with observations were studied earlier. For instance, some problems may be alleviated if the injection of energy happens on the large scale, the eddies are huge, and the corresponding timescales are much longer (see Lazarian 1999). The fact that the turbulence decays according to a power law, rather than exponentially, also helps. Indeed, if turbulent energy decays as t^{-1} , as suggested by Mac Low, Klessen, & Burkert (1998), a substantial level of turbulence should persist after 4–5 turnover times.

There is, however, another property of astrophysical turbulence related to the peculiar nature of the energy injection. It is accepted that sources of interstellar turbulence are localized. As a result, there is a substantial imbalance between the ingoing and outgoing energy flux surrounding every source. Below, we consider the effect of this imbalance on the turbulence decay timescale.

For an imbalanced turbulence, it is useful to consider the Elsasser variables, $z^\pm = \mathbf{v} \pm \mathbf{b}$, which describe wave packets

traveling in opposite directions along the magnetic field lines. Imbalanced turbulence means that wave packets traveling in one direction (say, z^+) have significantly larger amplitudes than the other. In astronomy, many energy sources are localized. For example, supernova explosions and OB winds are typical point energy sources. Furthermore, astrophysical jets from young stellar objects are believed to be highly collimated. With these localized energy sources, it is natural to think that interstellar turbulence is typically imbalanced. In fact, the concept of an imbalanced cascade is not new. Earlier papers (e.g., Matthaeus, Goldstein, & Montgomery 1983; Ting, Matthaeus, & Montgomery 1986; Ghosh, Matthaeus, & Montgomery 1988) have addressed the role and evolution of cross-helicity ($\equiv \mathbf{v} \cdot \mathbf{b}$). Since $4\langle \mathbf{v} \cdot \mathbf{b} \rangle = \langle (z^+)^2 \rangle - \langle (z^-)^2 \rangle$, nonzero cross-helicity implies an imbalanced turbulent cascade. These works, however, were mainly concerned with the growth of imbalance in decaying turbulence. Ghosh et al. (1988) investigated the evolution of cross-helicity and various spectra in driven turbulence. Hossain et al. (1995) discussed the effects of cross-helicity and energy difference $D = \langle v^2 \rangle - \langle b^2 \rangle$ on the decay of turbulence. Their low-resolution three-dimensional numerical simulations show the effect of cross-helicity, although that effect is not very conspicuous. A further study of imbalanced turbulence was given in MG01, who also suggested a connection between spontaneous appearance of local imbalance in the turbulent cascade and intermittency in MHD turbulence.

In this subsection, we explicitly relate the degree of imbalance and the decay timescale of turbulence in the presence of a strong uniform background field.

In Figure 7, we demonstrate that an imbalanced cascade does extend the lifetime of MHD turbulence. We use the run 144H-B₀1 to investigate the decay timescale. We ran the simulation up to $t = 75$, with nonzero driving forces. Then, at $t = 75$, we turned off the driving forces and let the turbulence decay. At $t = 75$, there is a slight imbalance between upward and downward moving components ($E_+ = 0.499$ and $E_- = 0.40$). This results from a natural fluctuation in the simulation. The case of $(E_+)_{t_0} = 0.8(E_-)_{t_0}$ corresponds to the simulation that starts off from this initial imbalance. In other cases, we either increase or decrease the energy of z^- components and, by turning off the forcing terms, let the turbulence decay. We can clearly observe that imbalanced turbulence extends the decay timescale substantially. Note that we normalized the initial energy to 1. The y-axis is the total (= up + down) energy.

In the right panel of Figure 7, we replot the left panel of Figure 7 in log-log scale. For the balanced case (i.e., zero cross-helicity case; *solid curve*), the energy decay follows a power law $E(t) \propto t^\alpha$, where α is very close to 1. This result is consistent with the previous three-dimensional result by Hossain et al. (1995). Note that hydrodynamic turbulence decays faster than this. For example, Kolmogorov turbulence decays as $E(t) \propto t^{-10/7}$. In this sense, it may not be absolutely correct to say that both hydro- and MHD turbulence decay within one eddy turnover time. However, note that the power law does not hold true from the beginning of decay. We believe that at the initial stage of decay, the speed of decay is still roughly proportional to the large-scale eddy turnover rate.

How far does a wave packet travel when there is an imbalance? Consider the equations governing an imbalanced cascade. From the MHD equations, Hossain et al.

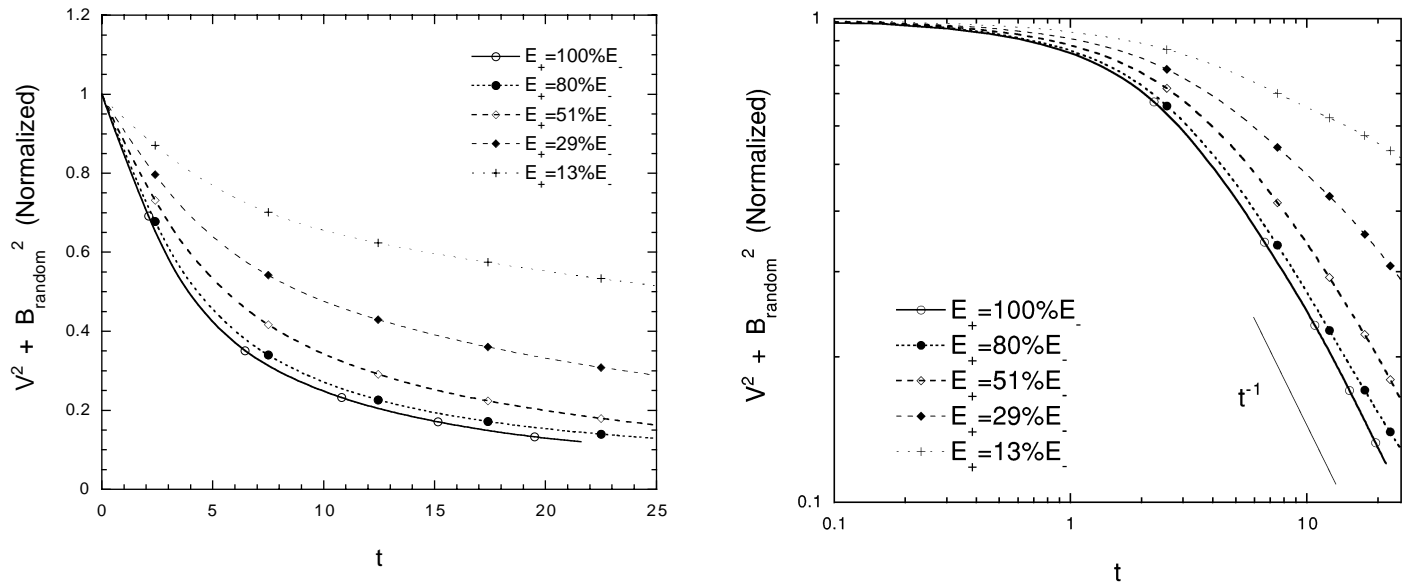


FIG. 7.—*Left*: Decay of unbalanced turbulence for run 144H-B₀1. An imbalanced cascade can extend decay time. It is clear that the decay of turbulence depends on the degree of imbalance. *Right*: Same as the left panel, but log-log scale. Note that about 3 time units is one eddy turnover time.

(1995) and MG01 derived a simple dynamical model for imbalanced turbulence. For decaying turbulence, they found

$$\frac{dE_+}{dt} = -\frac{E_+ E_-^{1/2}}{L}, \quad (26)$$

$$\frac{dE_-}{dt} = -\frac{E_- E_+^{1/2}}{L}, \quad (27)$$

where L is the largest energy-containing eddy scale.⁵ From these coupled equations, they showed that imbalance grows exponentially in decaying turbulence. Now let us consider a large-amplitude wave packet traveling in an already (weakly) turbulent background medium. Suppose that the large-amplitude wave packet corresponds to z^+ . Using the simplified equations, we obtain $\dot{E}_+/E_+ = -E_-^{1/2}/L$. If the background turbulence has a constant amplitude, the z^+ wave decays exponentially. It can travel

$$v^+ \Delta t \sim (E_+^{1/2}/E_-^{1/2})L, \quad (28)$$

where we use $v^+ \sim E_+^{1/2}$. This means that the wave packet can travel a long distance when imbalance is large (i.e., $E_+^{1/2} \gg E_-^{1/2}$). In real astrophysical situations, the problem is not as simple as this. Instead, the wave packet and the background turbulence can have different length scales (as opposed to the single scale L in the equations). We also need to consider the fact that the amplitude of the background turbulence does not stay constant and the front of the wave packet decays faster than the tail of the packet. Finally, MHD turbulence can influence the pressure support only if turbulent motions are at least comparable to the sound speed, which obviously requires a fully compressible treatment. Preliminary calculations with a compressible code (J. Cho & A. Lazarian, in preparation) show marginal coupling of compressible and incompressible

motions, while the development of the parametric instability (Fukuda & Hanawa 1999) requires more time to develop. We plan to investigate these possibilities in the future.

In this section, we found that turbulence decay time can be slow. This finding is very important for many astrophysical problems.

6. DISCUSSION

How relevant are our calculations for the “big picture”? First of all, they provide more support for the GS95 theory, indicating that for the first time, we have an adequate, if approximate, theory of MHD turbulence. Second, they extend the theory by treating new cases, e.g., an imbalanced cascade. Third, they establish new scaling relations and determine critical parameters, e.g., the functional form of g in equation (11), that will allow the theory to be applied to various astrophysical circumstances.

Our calculations are made within an intentionally simplified model, which is based on the physics of an incompressible fluid. This surely raises the question of the applicability of our scaling relations and conclusions to realistic circumstances. There are situations in which our scalings should be applicable. For instance, turbulence at very small scales is small amplitude, and therefore essentially incompressible. Processes that depend on the fine structure of turbulence, such as the scintillation, reconnection, and propagation of cosmic rays of moderate energies should be well described using our results.

If we consider the interstellar medium at larger scales, it is definitely compressible and has a whole range of energy injection/dissipation scales (see Scalo 1987), and the relative roles of vortical versus compressible motions are unclear. Nevertheless, we believe that our simplified treatment may still elucidate some of the basic processes. To what extent this claim can be justified will be clear when we compare compressible and incompressible results. However, if we accept that fast and slow MHD modes are subjected to fast collisionless damping (see Minter & Spangler 1997), the remaining modes are incompressible Alfvén modes. Those

⁵ For our current purposes, this simple system of equations is enough. For more rigorous equations on the evolution of $E_{\pm}(k)$, readers can refer to earlier closure equations, e.g., Grappin et al. 1982. See also Hossain et al. 1995 for time evolution of L .

should be well described by our model when turbulence is supersonic, but sub-Alfvénic. Our preliminary results (J. Cho & A. Lazarian, in preparation) show that the coupling of the modes is marginal, even in the compressible regime. Incidentally, recent studies of turbulence of H I in both our Galaxy and the SMC (Lazarian 1999; Lazarian & Pogosyan 2000; Stanimirovic & Lazarian 2001) show spectra of velocity and density consistent with the Kolmogorov scalings.⁶

Our approach is complementary to MG01. They studied turbulence in the regime where the magnetic energy is substantially larger than the kinetic energy at the energy-injection scale. Physically, their regime better reflects the properties of turbulence on small scales, at which the magnetic energy is indeed dominant. In our calculations, the kinetic energy is equal to the magnetic energy at the energy-injection scale, and therefore they reflect, for instance, what is happening in the interstellar medium at large scales. Our results show that even on those scales, GS95 scaling is applicable. This suggests that the astrophysical turbulence may be well tested not only via scintillations, which reflect properties of the turbulence on small scales, but with other techniques, e.g., synchrotron emission.

7. SUMMARY

Our findings can be summarized as follows:

The energy cascade timescale at a length scale l ($\sim 1/k$) is proportional to $l^{2/3}$ ($k^{-2/3}$), which is consistent with the prediction of the GS95 model and numerical simulations by MG01, who used a different method for obtaining this scaling. In this respect, MHD turbulence is similar to hydrodynamic turbulence. This scaling is distinctly different from the prediction of Iroshnikov-Kraichnan theory, $t_{\text{cas}} \propto l^{1/2}$.

⁶ If density acts as a passive scalar, its spectrum mimics that of velocity over the inertial range.

We found that velocity fluctuations in the direction parallel to the local magnetic field follow a similar scaling for both Alfvénic and pseudo-Alfvénic modes. We determined that parallel motions due to pseudo-Alfvén perturbations obey the scaling $v_{\parallel} \sim k_{\parallel}^{1/2}$. This finding is important for practical applications, e.g., for description of dust-grain motion.

To study intermittency, we calculated higher order longitudinal velocity structure functions in directions perpendicular to the local mean magnetic field and found that the scaling exponents are close to $\zeta_p^{\text{SL}} = p/9 + 2[1 - (2/3)^{p/3}]$. As this coincides with the She-Leveque model of intermittency in hydrodynamic flow, we speculate that there may be more similarities between magnetized and unmagnetized turbulent flows than has been previously anticipated.

We obtained correlation tensors that provide a good fit for our numerical results. These tensors are valuable for theoretical applications, e.g., for describing cosmic-ray transport.

We found that the rate at which MHD turbulence decays depends on the degree of energy imbalance between wave packets traveling in opposite directions. A substantial degree of imbalance can substantially extend the decay timescale of the MHD turbulence and the distance the turbulence can propagate from the source.

The authors are thankful to Peter Goldreich for attracting our attention to the case of imbalanced cascade and for many valuable discussions. We also thank John Mathis for many useful suggestions and discussions. A. L. and J. C. acknowledge the support of NSF Grant AST-0125544, and E. V. acknowledges the support of NSF Grant AST00-98615. This work was partially supported by National Computational Science Alliance under CTS 980010N and AST 000010N and utilized the NCSA SGI/CRAY Origin2000.

REFERENCES

- Barnes, A. 1966, *Phys. Fluids*, 9, 1483
 Bhattacharjee, A., Ng, C. S., & Spangler, S. R. 1998, *ApJ*, 494, 409
 Biskamp, D., & Schwarz, E. 2001, *Phys. Plasmas*, 8, 3282
 Borue, V., & Orszag, S. A. 1996, *J. Fluid Mech.*, 306, 293
 Castaing, B., Gagne, Y., & Hopfinger, E. 1990, *Physica D*, 46, 177
 Chandrasekhar, S. 1951, *Proc. R. Soc. London A*, 207, 301
 Cho, J., & Vishniac, E. T. 2000a, *ApJ*, 539, 273 (CV00)
 ———, 2000b, *ApJ*, 538, 217
 Fukuda, N., & Hanawa, T. 1999, *ApJ*, 517, 226
 Galtier, S., Nazarenko, S., Newell, A., & Pouquet, A. 2000, *J. Plasma Phys.*, 63, 447
 Ghosh, S., Matthaeus, W. H., & Montgomery, D. C. 1988, *Phys. Fluids*, 31, 2171
 Goldreich, P., & Sridhar, H. 1995, *ApJ*, 438, 763 (GS95)
 ———, 1997, *ApJ*, 485, 680
 Grappin, R., Frisch, U., Pouquet, A., & Leorat, J. 1982, *A&A*, 105, 6
 Hossain, M., Gray, P. C., Pontius, D. H., & Matthaeus, W. H. 1995, *Phys. Fluids*, 7, 2886
 Iroshnikov, P. 1963, *Astron. Zh.*, 40, 742 (English transl. in *Sov. Astron.*, 7, 566 [1964])
 Kolmogorov, A. 1941, *Dokl. Akad. Nauk SSSR*, 31, 538
 Kóta, J., & Jokipii, J. R. 2000, *ApJ*, 531, 1067
 Kraichnan, R. 1965, *Phys. Fluids*, 8, 1385
 Lazarian, A. 1995, *A&A*, 293, 507
 ———, 1999, in *Plasma Turbulence and Energetic Particles in Astrophysics*, ed. M. Ostrowski & R. Schlickeiser (Kraków: Obs. Astron., Univ. Jagiellonski), 28
 Lazarian, A., & Pogosyan, D. 2000, *ApJ*, 537, 720
 Lazarian, A., & Vishniac, E. T. 1999, *ApJ*, 517, 700
 Leamon, R. J., Smith, C. W., Ness, N. F., & Matthaeus, W. H. 1998, *J. Geophys. Res.*, 103, 4775
 Mac Low, M. 1999, *ApJ*, 524, 169
 Mac Low, M., Klessen, R., & Burkert, A. 1998, *Phys. Rev. Lett.*, 80, 2754
 Maron, J., & Goldreich, P. 2001, *ApJ*, 554, 1175 (MG01)
 Matthaeus, W. H., & Goldstein, M. L. 1982, *J. Geophys. Res.*, 87, 6011
 Matthaeus, W. H., Goldstein, M. L., & Montgomery, D. C. 1983, *Phys. Rev. Lett.*, 51, 1484
 Matthaeus, W. H., Oughton, S., Ghosh, S., & Hossain, M. 1998, *Phys. Rev. Lett.*, 81, 2056
 McKee, C. F. 1999, in *The Origin of Stars and Planetary Systems*, ed. J. L. Charles & D. K. Nikolaos (Dordrecht: Kluwer), 29
 Milano, L. J., Matthaeus, W. H., Dmitruk, P., & Montgomery, D. C. 2001, *Phys. Plasmas*, 8, 2673
 Minter, A., & Spangler, S. 1997, *ApJ*, 485, 182
 Montgomery, D. C. 1982, *Phys. Scr.*, 2, 83
 Montgomery, D. C., & Matthaeus, W. H. 1995, *ApJ*, 447, 706
 Montgomery, D. C., & Turner, L. 1981, *Phys. Fluids*, 24, 825
 Müller, W.-C., & Biskamp, D. 2000, *Phys. Rev. Lett.*, 84, 475
 Myers, P. C. 1999, in *The Origin of Stars and Planetary Systems*, ed. J. L. Charles & D. K. Nikolaos (Dordrecht: Kluwer), 67
 Ng, C. S., & Bhattacharjee, A. 1996, *ApJ*, 465, 845
 Oughton, S., Radler, K.-H., Matthaeus, W. H. 1997, *Phys. Rev. E*, 56, 2875
 Politano, H., & Pouquet, A. 1995, *Phys. Rev. E*, 52, 636
 Politano, H., Pouquet, A., & Carbone, V. 1998, *Europhys. Lett.*, 43, 516
 Politano, H., Pouquet, A., & Sulem, P. L. 1995, *Phys. Plasmas*, 2, 2931
 Rosenbluth, M. N., Monticello, D. A., Strauss, H. R., & White, R. B. 1976, *Phys. Fluids*, 19, 1987
 Scalo, J. M. 1987, in *Interstellar Processes*, ed. D. J. Hollenbach & H. A. Thronson (Dordrecht: Reidel), 349
 Schlickeiser, R. 1994, *ApJS*, 90, 929
 She, Z.-S., & Leveque, E. 1994, *Phys. Rev. Lett.*, 72, 336 (SL94)
 Shebalin, J. V., Matthaeus, W. H., & Montgomery, D. C. 1983, *J. Plasma Phys.*, 29, 525
 Sridhar, H., & Goldreich, P. 1994, *ApJ*, 432, 612
 Stanimirovic, S., & Lazarian, A. 2001, *ApJ*, 551, L53
 Strauss, H. R. 1976, *Phys. Fluids*, 19, 134
 Ting, A., Matthaeus, W. H., & Montgomery, D. C. 1986, *Phys. Fluids*, 29, 3261
 Zank, G. P., & Matthaeus, W. H. 1992, *J. Plasma Phys.*, 48, 85